Structural topology optimization in linear and nonlinear elasticity using a discontinuous Galerkin finite element method[*]

by

Yixin Tan[a,b], Lingkang Yan[a] and Shengfeng Zhu[a,c]

[a]School of Mathematical Sciences, East China Normal University,
Shanghai 200241, China
[b]Systems Research Institute, Polish Academy of Sciences,
ul. Newelska 6, 01-447, Warsaw, Poland
[c]Key Laboratory of MEA (Ministry of Education) & Shanghai Key
Laboratory of PMMP, East China Normal University, Shanghai 200241, China
e-mails: Yixin Tan: 52265500020@stu.ecnu.edu.cn
Lingkang Yan: 51255500070@stu.ecnu.edu.cn
Shengfeng Zhu: sfzhu@math.ecnu.edu.cn (corresponding author)

Abstract: A discontinuous Galerkin finite element method is developed for structural topology optimization with the level set method. The discontinuous Galerkin finite element method is employed to discretize and solve both the elasticity system, possible adjoint, and the transport equation of the level set function. Structural compliance and compliant mechanisms are considered for linear and nonlinear elastic structures. Numerical examples are provided to verify the effectiveness of the algorithm presented.

Keywords: topology optimization, level set method, discontinuous Galerkin finite element method, compliance, compliant mechanism, nonlinear elasticity

1. Introduction

Structural shape and topology optimization of structures has successful applications in industrial and engineering designs. The classical methods, based

---

on sensiti-vity analysis for shape and topology optimization, can be found in, e.g., Bendsoe and Sigmund (2003), Novotny and Sokolowski (2013), Novotny, Sokolowski and Zochowski (2019), or in the seminal work of Sokolowski and Zolésio (1992). In structural designs, e.g., compliance and compliant mechanism, the structure's geometry and material are required to be distributed in such a way that the structure remains as rigid/compliant as possible when stressed due to loads to improve its performance and stability. The design of a compliant mechanism, Howell (2001), often involves the optimization of structural shapes to achieve the required flexibility and adaptability, while maintaining sufficient strength and stability.

Most of the structural topology optimization models are based on the assumption of linear elasticity with small gradients of displacements (cf. Bendsoe and Sigmund, 2003). This assumption holds for a wide range of problems. However, the linearity assumption does not hold, due to the impact of nonlinear effects, in structural systems under the action of complex loads, see Buhl, Pedersen and Sigmund (2000), Ganghoffer, Plotnikov and Sokolowski (2018), Kwak and Cho (2005), Kim (2015). The stress-strain relationship may undergo nonlinear changes, such as bending, buckling, and other phenomena, which not only affect the performance and stability of the structure, but also pose new challenges to the analysis and design.

In this paper, we consider structural topology optimization of linear and non-linear elastic systems with minimal compliance and compliant mechanisms. Most traditional topology optimization methods are based on finite element analysis with continuous piecewise Lagrange polynomials. Discontinuous Galerkin finite element method (DGFEM) (Ern and Guermond, 2006; Hansbo and Larson, 2022; Rivière et al., 2003; Tan and Zhu, 2023) is an efficient technique for numerically solving partial differential equations. Different from the traditional finite element method, the DGFEM can use different discontinuous polynomials to approximate the solution in each mesh element of the domain. This implies that the approximate solution will typically be discontinuous between adjacent elements. DGFEM (Arnold et al., 2002) usually refers to the weak forms of integration to establish discrete equations, and introduces numerical fluxes to deal with solution discontinuities between mesh elements. These characteristics make the DGFEM advantageous in dealing with problems in the fields of fluid dynamics, elasticity, electromagnetics, etc. In addition, the DGFEM's advantages of high-order accuracy, adaptability, and parallelism allow it to be an important choice for solving complex partial differential equations. Therefore, we adopted the DGFEM for topology optimization. In Evgrafov (2018), discon-

tinuous Petrov–Galerkin methods were used in solving linear elastic systems for topology optimization with the SIMP method. In Adams, Giani and Coombs (2016), a level set method was proposed for topology optimization of structural compliance with discontinuous Galerkin symmetric interior penalty finite element method, Arnold et al. (2002), for spatial discretizations of linear elasticity system and level set function.

In this paper, we develop a DGFEM for structural topology optimization with a level set method. In both stages of state analysis and design, we use the DGFEM for discretizations of linear/nonlinear elasticity and transport equation of the level set function. The level set method, originally used for interface tracking, Osher and Sethian (1988), has been developed as a popular boundary variational topology optimization technique (see, e.g., Allaire et al., 2005; Allaire, Jouve and Toader, 2004; Fulmanski et al., 2008; Qian and Zhu, 2022; Tan and Zhu, 2014; Zheng, Zhu and Soleymani, 2024; or Zhu, Hu and Wu, 2018). Our methodology not only has the level set method's advantages, such as shape and topological change mechanism on fixed design regions, but also has DGFEM's high-order accuracy, adaptability, parallelism, etc.

The rest of the paper is organized as follows. In Section 2, the model formulations of structural topology optimization are introduced for linear and nonlinear elasticity. Compliance minimization and compliant mechanisms are considered. In Section 3, shape sensitivity analysis is presented. In Section 4, DGFEM for discretizations of both linear and nonlinear elasticity are introduced. In Section 5, we introduce the topology optimization algorithm of level set type using the DGFEM. In Section 6, numerical results are presented. Brief conclusions follow.

2. Structural topology optimization

In this section, we introduce the problem of structural topology optimization with linear elasticity and nonlinear elasticity.

2.1. Linear elasticity

Let $\Omega \subset \mathbb{R}^d$ ($d = 2, 3$) be an open bounded domain with isotropic elastic material and Lipschitz continuous boundary $\partial\Omega$, which consists of non-intersecting boundaries Γ_D, Γ_N, and Γ. Let external loads $\boldsymbol{f} : \Omega \to \mathbb{R}^d$ and $\boldsymbol{g} : \Gamma_N \to \mathbb{R}^d$ be a body force intensity and a surface traction, respectively. They are independent

of deformation. Consider linear elasticity system with displacement $\boldsymbol{u} : \Omega \to \mathbb{R}^d$:

$$\begin{cases} -\mathrm{div}\,\boldsymbol{\sigma} = \boldsymbol{f} & \text{in } \Omega, \\ \boldsymbol{u} = \boldsymbol{0} & \text{on } \Gamma_{\mathrm{D}}, \\ \boldsymbol{\sigma}\boldsymbol{n} = \boldsymbol{g} & \text{on } \Gamma_{\mathrm{N}}, \\ \boldsymbol{\sigma}\boldsymbol{n} = \boldsymbol{0} & \text{on } \Gamma, \end{cases} \tag{1}$$

where $\boldsymbol{n}$ is an outward unit normal vector, the stress tensor $\boldsymbol{\sigma} = \boldsymbol{\sigma}(\boldsymbol{u})$ satisfies Hooke's law

$$\boldsymbol{\sigma} = \lambda \,\mathrm{Tr}\,(\boldsymbol{\varepsilon})I + 2\mu\boldsymbol{\varepsilon},$$

with μ and λ being the Lamé parameters, Tr being the trace operator, I being the identity matrix, and the strain tensor

$$\boldsymbol{\varepsilon} = \frac{1}{2}(\mathrm{D}\boldsymbol{u} + \mathrm{D}\boldsymbol{u}^T). \tag{2}$$

We consider the minimization of the compliance

$$J(\Omega) = \int_{\Omega} \boldsymbol{f} \cdot \boldsymbol{u}\mathrm{d}x + \int_{\Gamma_{\mathrm{N}}} \boldsymbol{g} \cdot \boldsymbol{u}\mathrm{d}s \tag{3}$$

subject to a volume constraint. This constraint is simply aggregated to the objective, so that the problem is described as

$$\min_{\Omega}\{J(\Omega) + \ell\,\mathrm{Vol}(\Omega)\},$$

where $\ell > 0$ is a fixed Lagrange multiplier and $\mathrm{Vol}(\Omega)$ denotes the Lebesgue measure of Ω.

The next model to consider is the compliant mechanism, which is intriguing, due to its significant practical implications. The setting is that of an inverter mechanism (Howell, 2001; Novotny, Sokolowski and Zochowski, 2019) introduced to simulate the reciprocal interaction between a workpiece and the mechanism. The displacement inverter converts an input displacement on the left edge to a displacement in the opposite direction on the right edge. The setting is that of a force inverter, as depicted in Fig. 1. The considered shapes are contained inside a 1×1 two-dimensional box D; they are fixed at their upper and lower left corners, while a horizontal load is applied at the center of their left-hand side. Our aim is that the horizontal displacement of the structure at the center of their right-hand side be as negative as possible. Denote by Γ_{out}
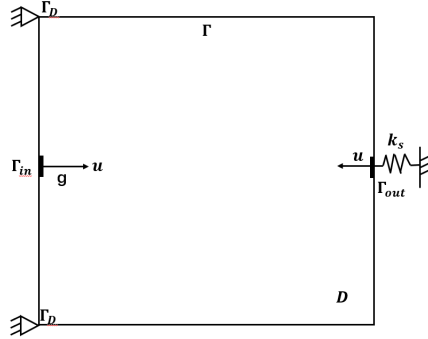
Figure 1: Design domain of inverter

and Γ_{in} the output and input boundaries, respectively. An artificial spring with stiffness $k_s > 0$ is attached at the output Γ_{out} to simulate the resistance of a workpiece.

Let $\Omega \subset D \subset \mathbb{R}^d$ $(d = 2, 3)$, where D is a fixed domain, whose boundary ∂D is partitioned into four subsets $\Gamma_D, \Gamma_{\text{in}}, \Gamma_{\text{out}}$ and Γ. Homogeneous Dirichlet and Neumann boundary conditions are imposed on Γ_D and Γ, respectively. On Γ_{in}, a non-homogeneous Neumann condition is imposed with a surface load $g \in H^{-1/2} (\Gamma_{\text{in}})^d$. The free interface between the weak and strong phase is $\partial \Omega$. A spring with stiffness k_s is connected to the boundary Γ_{out}, which corresponds to a Robin boundary condition used for the mechanism. Define a space

$$\mathbf{V} := \left\{ \boldsymbol{v} \in \boldsymbol{H^1}(\Omega) : \boldsymbol{v} = \boldsymbol{0} \text{ on } \Gamma_D \right\},$$

where $\boldsymbol{H^1}(\Omega) := H^1(\Omega)^d$ with $H^1(\Omega) = \{v \in L^2(\Omega) \,|\, \partial_i v \in L^2(\Omega), \, i = 1, \cdots, d\}$.

Let a displacement field $\boldsymbol{u} \in \mathbf{V}$ be the solution of the linear elasticity system

$$\begin{cases} -\operatorname{div} \boldsymbol{\sigma} = \boldsymbol{0} & \text{in } \Omega, \\ \quad\;\; \boldsymbol{u} = \boldsymbol{0} & \text{on } \Gamma_D, \\ \quad\;\; \boldsymbol{\sigma n} = \boldsymbol{g} & \text{on } \Gamma_{\text{in}}, \\ \quad\;\; \boldsymbol{\sigma n} = \boldsymbol{0} & \text{on } \Gamma, \\ \quad\;\; \boldsymbol{\sigma n} = -k_s \boldsymbol{u} & \text{on } \Gamma_{\text{out}}, \end{cases} \tag{4}$$

In order to maximize output displacement and limit input displacement, we minimize the cost functional $(d = 2)$

$$J(\Omega) := \int_{\Gamma_{\text{in}}} \eta_{\text{in}} \, u_1 \mathrm{d}s + \int_{\Gamma_{\text{out}}} \eta_{\text{out}} \, u_1 \mathrm{d}s \tag{5}$$

with $\boldsymbol{u} = (u_1, u_2)$ and constants $\eta_{\text{in}}, \eta_{\text{out}} > 0$. Note that $u_1 > 0$ on Γ_{in} and $u_1 < 0$ on Γ_{out}. The variational formulation of (4) consists in finding $u \in \mathbf{V}$ such that

$$\int_\Omega \boldsymbol{\sigma}(\boldsymbol{u}) : \boldsymbol{\varepsilon}(\boldsymbol{v}) \mathrm{d}x + \int_{\Gamma_{\text{out}}} k_s \boldsymbol{u} \cdot \boldsymbol{v} \mathrm{d}s = \int_{\Gamma_{\text{in}}} \boldsymbol{g} \cdot \boldsymbol{v} \mathrm{d}s \quad \forall \boldsymbol{v} \in \mathbf{V}. \tag{6}$$

2.2. Nonlinear elasticity

Consider nonlinear elasticity with hyperelastic material and define strain energy

$$W(E) = \frac{1}{2} E : A : E, \tag{7}$$

where the Lagrangian strain

$$E = \frac{1}{2}(F^T F - I) = \frac{1}{2} \left(\mathrm{D}\boldsymbol{u}^{\mathrm{T}} + \mathrm{D}\boldsymbol{u} + \mathrm{D}\boldsymbol{u}^{\mathrm{T}} \mathrm{D}\boldsymbol{u} \right), \tag{8}$$

with F being the deformation gradient, written as

$$F = I + \mathrm{D}\boldsymbol{u}, \tag{9}$$

A is the fourth-order constitutive tensor for isotropic materials:

$$A = \lambda I \otimes I + 2\mu \mathbf{1}, \tag{10}$$

with $\mathbf{1}$ being defined as $\mathbf{1}_{ijkl} = (\delta_{ik}\delta_{jl} + \delta_{il}\delta_{jk})/2$. The second Piola–Kirchhoff stress tensor $\boldsymbol{T}$

$$\boldsymbol{T} \equiv \frac{\partial W(E)}{\partial E} = A : E = \lambda \operatorname{Tr}(E) I + 2\mu E. \tag{11}$$

Consider the following nonlinear elasticity problem for $\boldsymbol{u} \in \mathbf{V}$:

$$\begin{cases} -\operatorname{div} \boldsymbol{T}(\boldsymbol{u}) = \boldsymbol{f} & \text{in } \Omega, \\ \boldsymbol{u} = \mathbf{0} & \text{on } \Gamma_{\text{D}}, \\ \boldsymbol{T}(\boldsymbol{u})\boldsymbol{n} = \boldsymbol{g} & \text{on } \Gamma_{\text{N}}, \\ \boldsymbol{T}(\boldsymbol{u})\boldsymbol{n} = \mathbf{0} & \text{on } \Gamma, \end{cases} \tag{12}$$

where $\boldsymbol{n}$ is an outward unit normal on the boundary. The potential energy of the nonlinear elastic system is the difference between the stored strain energy and the work done by external forces:

$$\Pi(\boldsymbol{u}) = \int_\Omega W(E) \, \mathrm{d}x - \int_\Omega \boldsymbol{f} \cdot \boldsymbol{u} \, \mathrm{d}x - \int_{\Gamma_N} \boldsymbol{g} \cdot \boldsymbol{u} \, \mathrm{d}s. \tag{13}$$

The principle of minimum potential energy holds in the sense that the displacement field in the equilibrium minimizes (13).

For finding the displacement at the minimum potential energy, a perturbation method is used. Let us assume that the displacement field $\boldsymbol{u}$ is perturbed in a direction $\boldsymbol{\psi} \in \boldsymbol{V}$. The perturbed displacement is $\boldsymbol{u}_t = \boldsymbol{u} + t\boldsymbol{\psi}$, where $t > 0$ is the parameter that controls the perturbation size. Then, the first variation of the potential energy at the equilibrium state for any direction $\boldsymbol{\psi}$ implies that

$$
\begin{aligned}
0 &= \left. \frac{\mathrm{d}}{\mathrm{d}t} \Pi(\boldsymbol{u} + t\boldsymbol{\psi}) \right|_{t=0} \\
&= \int_\Omega \frac{\partial W(E)}{\partial E} : \left. \frac{\mathrm{d}E(\boldsymbol{u} + t\boldsymbol{\psi})}{\mathrm{d}t} \right|_{t=0} \mathrm{d}x - \int_\Omega \boldsymbol{f} \cdot \boldsymbol{\psi}\mathrm{d}x - \int_{\Gamma_N} \boldsymbol{g} \cdot \boldsymbol{\psi}\mathrm{d}s, \\
&= \int_\Omega \boldsymbol{T}(\boldsymbol{u}) : \hat{E}(\boldsymbol{u}, \boldsymbol{\psi})\mathrm{d}x - \int_\Omega \boldsymbol{f} \cdot \boldsymbol{\psi}\mathrm{d}x - \int_{\Gamma_N} \boldsymbol{g} \cdot \boldsymbol{\psi}\mathrm{d}s,
\end{aligned} \tag{14}
$$

where $\boldsymbol{T}(\boldsymbol{u}) = A : E(\boldsymbol{u})$ and

$$
\hat{E}(\boldsymbol{u}, \boldsymbol{\psi}) := \left. \frac{\mathrm{d}E(\boldsymbol{u} + t\boldsymbol{\psi})}{\mathrm{d}t} \right|_{t=0} = \mathcal{S}(F\mathrm{D}\boldsymbol{\psi}) \tag{15}
$$

with $\mathcal{S}$ being a matrix's symmetrical part, i.e., $\mathcal{S}(M) = (M + M^T)/2$ for every matrix M. Thus, (14) has a variational form:

$$
a(\boldsymbol{u}, \boldsymbol{\psi}) = l(\boldsymbol{\psi}) \quad \forall \, \boldsymbol{\psi} \in \boldsymbol{V}, \tag{16}
$$

where

$$
a(\boldsymbol{u}, \boldsymbol{\psi}) = \int_\Omega A : E(\boldsymbol{u}) : \hat{E}(\boldsymbol{u}, \boldsymbol{\psi}) \, \mathrm{d}x,
$$

and

$$
l(\boldsymbol{\psi}) = \int_\Omega \boldsymbol{f} \cdot \boldsymbol{\psi} \, \mathrm{d}x + \int_{\Gamma_N} \boldsymbol{g} \cdot \boldsymbol{\psi} \, \mathrm{d}s.
$$

Consider the minimization problem

$$
\min_\Omega \{ J(\Omega) = -\Pi(\boldsymbol{u}) + \ell \, \mathrm{Vol}(\Omega) \},
$$

where $\Pi(\boldsymbol{u})$ is defined in (13) and ℓ is a fixed Lagrange multiplier.

Consider the following nonlinear elasticity problem in the compliant mechanism model:

$$\begin{cases} -\mathrm{div}\,\boldsymbol{T}(\boldsymbol{u}) = \boldsymbol{f} & \text{in } \Omega, \\ \quad\quad\quad \boldsymbol{u} = \boldsymbol{0} & \text{on } \Gamma_\mathrm{D}, \\ \quad \boldsymbol{T}(\boldsymbol{u})\boldsymbol{n} = \boldsymbol{g} & \text{on } \Gamma_\mathrm{in}, \\ \quad \boldsymbol{T}(\boldsymbol{u})\boldsymbol{n} = \boldsymbol{0} & \text{on } \Gamma, \\ \quad \boldsymbol{T}(\boldsymbol{u})\boldsymbol{n} = -k_s\boldsymbol{u} & \text{on } \Gamma_\mathrm{out}, \end{cases} \tag{17}$$

We also consider minimizing the cost functional (5). For the state, consider finding of $\boldsymbol{u} \in \mathbf{V}$ such that

$$\int_\Omega A : E(\boldsymbol{u}) : \hat{E}(\boldsymbol{u}, \boldsymbol{\psi}) \, \mathrm{d}x + \int_{\Gamma_\mathrm{out}} k_s \boldsymbol{u}\cdot\boldsymbol{\psi} \, \mathrm{d}s = \int_\Omega \boldsymbol{f}\cdot\boldsymbol{\psi} \, \mathrm{d}x + \int_{\Gamma_\mathrm{in}} \boldsymbol{g}\cdot\boldsymbol{\psi} \, \mathrm{d}s \quad \forall \boldsymbol{\psi} \in \mathbf{V}. \tag{18}$$

3. Shape sensitivity analysis

Shape sensitivity analysis based on shape calculus is a valuable tool for designing numerical methods for shape optimization. We use the perturbation of identity method, which is equivalent to the velocity method and the method of mapping in the sense of first-order Taylor expansion. For $t \in [0, \varepsilon_1)\,(\varepsilon_1 > 0)$, define a family of smooth mappings $\{F_t\}_{t\in[0,\varepsilon_1)}$ with $F_t : \bar{D} \to \bar{D}$. The boundary Γ_D is fixed, i.e., $F_t\,(\Gamma_D) = \Gamma_D$. Then, we denote $\Omega_t := F_t(\Omega) = \{F_t(\boldsymbol{x}) : \boldsymbol{x} \in \Omega\}$ with $\Omega_0 = \Omega$ and the boundary $\partial\Omega_t := F_t(\partial\Omega) = \{F_t(\boldsymbol{x}) : \boldsymbol{x} \in \partial\Omega\}$ with $\partial\Omega_0 = \partial\Omega$. The mappings $\{F_t\}_{t\in[0,\varepsilon_1)}$ describe the motion of each point in D, i.e., at $t \in [0, \epsilon_1]$, the point $\boldsymbol{x} \in D$ has a new position $\boldsymbol{x}_t := F_t(\boldsymbol{x}) \in D$ with $\boldsymbol{x}_0 = \boldsymbol{x}$. More specifically,

$$F_t = \mathrm{Id} + t\boldsymbol{\theta},$$

where Id represents the identity mapping and $\boldsymbol{\theta} = \boldsymbol{\theta}(\boldsymbol{x})$ denotes a sufficiently smooth vector field in

$$\boldsymbol{\Theta}_{ad} = \left\{ \boldsymbol{\theta} \in W^{1,\infty}\left(D; \mathbb{R}^d\right) | \boldsymbol{\theta} = \boldsymbol{0} \text{ on } \Gamma_D \right\}.$$

Here, $W^{1,\infty}\left(D; \mathbb{R}^d\right)$ is the space of vector field functions, for which each of its components belongs to $W^{1,\infty}(D)$, a Banach space of functions uniformly bounded up to the first-order weak derivative. Define an admissible set of considered shapes:

$$\mathcal{U}_{ad} := \{\Omega \subset D \text{ is bounded and Lipschitz}\}.$$

DEFINITION 3.1 *For a real-valued shape functional $J : \Omega \mapsto \mathbb{R}$, a shape functional J is called shape differentiable at Ω, if*

$$dJ(\Omega; \boldsymbol{\theta}) := \lim_{t \searrow 0} \frac{J(\Omega_t) - J(\Omega)}{t} \tag{19}$$

exists for all directions $\boldsymbol{\theta}$ and the mapping $\boldsymbol{\theta} \mapsto dJ(\Omega; \boldsymbol{\theta})$ is linear and continuous. The expression $dJ(\Omega; \boldsymbol{\theta})$ is called an Eulerian derivative of J at Ω in direction $\boldsymbol{\theta}$.

LEMMA 3.1 (ALLAIRE, DAPOGNY AND JOUVE, 2021, SECTION 4) *Let Ω be a smooth bounded open set. Then for*

$$J(\Omega) = \int_{\Omega} f \mathrm{d}x \tag{20}$$

with $f = f(\boldsymbol{x}) \in W^{1,1}\left(\mathbb{R}^d\right)$, J is differentiable at Ω and for any $\boldsymbol{\theta} \in W^{1,\infty}\left(D; \mathbb{R}^d\right)$

$$dJ(\Omega; \boldsymbol{\theta}) = \int_{\Omega} (\dot{f} + f \operatorname{div} \boldsymbol{\theta}) \mathrm{d}x, \tag{21}$$

in which $\dot{f} = \nabla f \cdot \boldsymbol{\theta}$. If, in addition, Ω is of class C^1, it holds that

$$dJ(\Omega; \boldsymbol{\theta}) = \int_{\partial\Omega} f \theta_n \mathrm{d}s, \tag{22}$$

where $\theta_n = \boldsymbol{\theta} \cdot \boldsymbol{n}$.

For the compliance problem of linear elasticity, we obtain from Laurain (2018, Section 3) the following distributed Eulerian derivative and thus omit proof for simplicity.

THEOREM 3.1 (COMPLIANCE IN LINEAR ELASTICITY) *Let Ω be an open bounded domain. Then $J(\Omega)$ is shape differentiable and the distributed type of Eulerian derivative of (5) reads:*

$$dJ(\Omega; \boldsymbol{\theta}) = \int_{\Omega} \left(2\mathrm{D}\boldsymbol{u}^T A\boldsymbol{\varepsilon}(\boldsymbol{u}) : \mathrm{D}\boldsymbol{\theta} - A\boldsymbol{\varepsilon}(\boldsymbol{u}) : \boldsymbol{\varepsilon}(\boldsymbol{u}) \operatorname{div} \boldsymbol{\theta}\right) \mathrm{d}x. \tag{23}$$

For shape sensitivity analysis of nonlinear elasticity, consider an objective

$$J(\boldsymbol{u}) = \int_{\Omega} j(\boldsymbol{u}) \, \mathrm{d}x + \int_{\Gamma_N} l(\boldsymbol{u}) \, \mathrm{d}s, \tag{24}$$

where $j(\cdot) : \mathbb{R}^d \to \mathbb{R}$ and $l(\cdot) : \mathbb{R}^d \to \mathbb{R}$ are C^1. We denote

$$\delta T = \frac{\partial T}{\partial E} : \delta E = A : \delta E, \tag{25}$$

where δT is the stress variation and δE is the strain variation. We note that the increment of deformation gradient is $\delta F = \mathrm{D}\delta\boldsymbol{u}$. Then, the increment of the Lagrangian strain and its variation can be obtained, respectively, as

$$\delta E(\boldsymbol{u}, \delta\boldsymbol{u}) = \mathcal{S}(F \cdot \mathrm{D}\delta\boldsymbol{u}), \qquad \delta\hat{E}(\delta\boldsymbol{u}, \boldsymbol{\psi}) = \mathcal{S}(\mathrm{D}\delta\boldsymbol{u} \cdot \mathrm{D}\boldsymbol{\psi}). \tag{26}$$

Introduce a Lagrangian with $\boldsymbol{v}, \boldsymbol{q} \in \mathbf{V}$

$$\mathcal{L}(\Omega, \boldsymbol{v}, \boldsymbol{q}) =$$
$$\int_{\Omega} j(\boldsymbol{v})\mathrm{d}x + \int_{\Gamma_N} l(\boldsymbol{v})\mathrm{d}s + \int_{\Omega} A : E(\boldsymbol{v}) : \hat{E}(\boldsymbol{v}, \boldsymbol{q})\mathrm{d}x - \int_{\Omega} \boldsymbol{f} \cdot \boldsymbol{q}\mathrm{d}x - \int_{\Gamma_N} \boldsymbol{g} \cdot \boldsymbol{q}\mathrm{d}s. \tag{27}$$

The first-order optimality condition implies for $\mathcal{L}$ at $(\boldsymbol{u}, \boldsymbol{p})$ in the direction $\boldsymbol{\psi} \in \mathbf{V}$ that

$$0 = \left\langle \frac{\partial}{\partial\boldsymbol{v}}\mathcal{L}(\Omega, \boldsymbol{u}, \boldsymbol{p}), \boldsymbol{\psi} \right\rangle$$
$$= \int_{\Omega} j'(\boldsymbol{u}) \cdot \boldsymbol{\psi}\mathrm{d}x + \int_{\Gamma_N} l'(\boldsymbol{u}) \cdot \boldsymbol{\psi}\mathrm{d}s + \int_{\Omega} \big(\delta T(\boldsymbol{u})\boldsymbol{\psi} : \hat{E}(\boldsymbol{u}, \boldsymbol{p}) + T(\boldsymbol{u})$$
$$: \delta\hat{E}(\boldsymbol{u}, \boldsymbol{p})\boldsymbol{\psi}\big)\mathrm{d}x$$
$$= \int_{\Omega} j'(\boldsymbol{u}) \cdot \boldsymbol{\psi}\mathrm{d}x + \int_{\Gamma_N} l'(\boldsymbol{u}) \cdot \boldsymbol{\psi}\mathrm{d}s + \int_{\Omega} \big(A : \delta\tilde{E}(\boldsymbol{u}, \boldsymbol{\psi}) : \hat{E}(\boldsymbol{u}, \boldsymbol{p}) + T(\boldsymbol{u})$$
$$: \delta\bar{E}(\boldsymbol{u}, \boldsymbol{p}, \boldsymbol{\psi}))\mathrm{d}x, \tag{28}$$

where we denote $\delta\tilde{E}(\boldsymbol{u}, \boldsymbol{\psi}) := \delta E(\boldsymbol{u})\boldsymbol{\psi}$ and $\delta\bar{E}(\boldsymbol{u}, \boldsymbol{p}, \boldsymbol{\psi}) := \delta\hat{E}(\boldsymbol{u}, \boldsymbol{p})\boldsymbol{\psi}$. Therefore, the weak form of the adjoint reads as

$$\int_{\Omega} \Big(A : \delta\tilde{E}(\boldsymbol{u}, \boldsymbol{\psi}) : \hat{E}(\boldsymbol{u}, \boldsymbol{p}) + T(\boldsymbol{u}) : \delta\bar{E}(\boldsymbol{u}, \boldsymbol{p}, \boldsymbol{\psi})\Big)\mathrm{d}x$$
$$= -\int_{\Omega} j'(\boldsymbol{u}) \cdot \boldsymbol{\psi}\mathrm{d}x - \int_{\Gamma_N} l'(\boldsymbol{u}) \cdot \boldsymbol{\psi}\mathrm{d}s, \quad \forall\ \psi \in \mathbf{V} \tag{29}$$

where $T = A : E$. Define

$$\mathbf{V}_t := \big\{\boldsymbol{v} \in \boldsymbol{H^1}(\Omega_t) : \boldsymbol{v} = \mathbf{0} \text{ on } \Gamma_D\big\}.$$

THEOREM 3.2 (COMPLIANCE IN NONLINEAR ELASTICITY) *Let Ω be an open bounded domain. Let $\boldsymbol{u}$ and $\boldsymbol{p}$ be weak solutions to (16) and (3) in nonlinear elasticity, respectively. Then, the distributed Eulerian derivative of (24) reads:*

$$dJ(\Omega; \boldsymbol{\theta}) = \int_{\Omega} \Big(A\partial_t\mathcal{E}(0, \boldsymbol{u}) : \mathscr{E}(0, \boldsymbol{u}, \boldsymbol{p}) + A\mathcal{E}(0, \boldsymbol{u}) : \partial_t\mathscr{E}(0, \boldsymbol{u}, \boldsymbol{p})$$

$$+A\mathcal{E}(0,\boldsymbol{u}) : \mathscr{E}(0,\boldsymbol{u},\boldsymbol{p})\operatorname{div}\boldsymbol{\theta} + \operatorname{div}(j(\boldsymbol{u})\boldsymbol{\theta}) - \operatorname{div}(\boldsymbol{f}\cdot\boldsymbol{p}\boldsymbol{\theta})\Big)\mathrm{d}x, \tag{30}$$

where

$$\partial_t\mathcal{E}(0,\boldsymbol{u}) = -\mathcal{S}(\mathrm{D}\boldsymbol{u}\mathrm{D}\boldsymbol{\theta}) - \mathcal{S}(\mathrm{D}\boldsymbol{\theta}^T\mathrm{D}\boldsymbol{u}^T\mathrm{D}\boldsymbol{u}), \tag{31}$$

$$\partial_t\mathscr{E}(0,\boldsymbol{u},\boldsymbol{p}) = -\mathcal{S}(\mathrm{D}\boldsymbol{p}\mathrm{D}\boldsymbol{\theta}) - \mathcal{S}(\mathrm{D}\boldsymbol{\theta}^T\mathrm{D}\boldsymbol{u}^T\mathrm{D}\boldsymbol{p}) - \mathcal{S}(\mathrm{D}\boldsymbol{u}^T\mathrm{D}\boldsymbol{p}\mathrm{D}\boldsymbol{\theta}), \tag{32}$$

$$\mathcal{E}(0,\boldsymbol{u}) = \mathcal{S}(\mathrm{D}\boldsymbol{u}) + \frac{1}{2}\mathrm{D}\boldsymbol{u}^T\mathrm{D}\boldsymbol{u}, \tag{33}$$

$$\mathscr{E}(0,\boldsymbol{u},\boldsymbol{v}) = \mathcal{S}\left(\mathrm{D}\boldsymbol{v} + \mathrm{D}\boldsymbol{v}^T\mathrm{D}\boldsymbol{u}\right). \tag{34}$$

If, moreover, Ω is sufficiently smooth, $J(\Omega)$ is shape differentiable and its boundary type of Eulerian derivative reads:

$$dJ(\Omega;\boldsymbol{\theta}) = \int_\Gamma (j(\boldsymbol{u}) + A : E(\boldsymbol{u}) : \hat{E}(\boldsymbol{u},\boldsymbol{p}) - \boldsymbol{f}\cdot\boldsymbol{p} + \ell)\theta_n\,\mathrm{d}s, \tag{35}$$

where $\theta_n = \boldsymbol{\theta}\cdot\boldsymbol{n}$.

PROOF We minimize the cost functional (24). The variational formulation of (12) is to find $\boldsymbol{u}\in\mathbf{V}$ such that

$$\int_\Omega A : E(\boldsymbol{u}) : \hat{E}(\boldsymbol{u},\boldsymbol{v})\,\mathrm{d}x = \int_\Omega \boldsymbol{f}\cdot\boldsymbol{v}\,\mathrm{d}x + \int_{\Gamma_N} \boldsymbol{g}\cdot\boldsymbol{v}\,\mathrm{d}s \quad \forall\boldsymbol{v}\in\mathbf{V}. \tag{36}$$

Denote by $\boldsymbol{u_t}$ the solution of (12) with Ω replaced by Ω_t. Let $\boldsymbol{u}^t = \boldsymbol{u}_t \circ T_t$ and use the chain rule to have

$$\mathrm{D}\boldsymbol{u}^t = \mathrm{D}\left(\boldsymbol{u}_t \circ T_t\right) = (\mathrm{D}\boldsymbol{u}_t) \circ T_t\mathrm{D}T_t. \tag{37}$$

Consequently,

$$\begin{aligned}\mathcal{E}\left(t,\boldsymbol{u}^t\right) :&= E\left(\boldsymbol{u}_t\right) \circ T_t = \frac{1}{2}\left(\mathrm{D}\boldsymbol{u}_t + \mathrm{D}\boldsymbol{u}_t{}^T + \mathrm{D}\boldsymbol{u}_t{}^T\mathrm{D}\boldsymbol{u}_t\right) \circ T_t \\ &= \mathcal{S}\left(\mathrm{D}\boldsymbol{u}^t\mathrm{D}T_t^{-1}\right) + \left[(\mathrm{D}T_t)^{-T}\left(\mathrm{D}\boldsymbol{u}^t\right)^T\right]\left[\mathrm{D}\boldsymbol{u}^t\left(\mathrm{D}T_t\right)^{-1}\right]/2.\end{aligned} \tag{38}$$

and

$$\begin{aligned}\mathscr{E}(t,\boldsymbol{u}^t,\boldsymbol{v}^t) :&= \hat{E}(\boldsymbol{u}_t,\boldsymbol{v}_t) \circ T_t = \frac{1}{2}\left(\mathrm{D}\boldsymbol{v}_t + \mathrm{D}\boldsymbol{v}_t{}^T + \mathrm{D}\boldsymbol{v}_t{}^T\mathrm{D}\boldsymbol{u}_t + \mathrm{D}\boldsymbol{u}_t{}^T\mathrm{D}\boldsymbol{v}_t\right) \circ T_t \\ &= \mathcal{S}\left(\mathrm{D}\boldsymbol{v}^t\mathrm{D}T_t^{-1}\right) + \mathcal{S}\left([(\mathrm{D}T_t)^{-T}(\mathrm{D}\boldsymbol{u}^t)^T][\mathrm{D}\boldsymbol{v}^t(\mathrm{D}T_t)^{-1}]\right).\end{aligned} \tag{39}$$

The variational formulation for the state on Ω_t is to find $\boldsymbol{u}_t \in \mathbf{V}_t$ such that

$$\int_{\Omega_t} A_{\Omega_t} : E(\boldsymbol{u}_t) : \hat{E}(\boldsymbol{u}_t, \boldsymbol{v}_t) \, \mathrm{d}x_t = \int_{\Omega_t} \boldsymbol{f} \cdot \boldsymbol{v}_t \, \mathrm{d}x_t + \int_{\Gamma_N} \boldsymbol{g} \cdot \boldsymbol{v}_t \, \mathrm{d}s_t \quad \forall \boldsymbol{v}_t \in \mathbf{V}_t. \tag{40}$$

Denote by $\xi(t) := \det \mathrm{D}T_t$ the determinant of the Jacobian of transformation. Note that neither the Jacobian nor T_t need to appear in the integrals on Γ_N and Γ, since we have assumed $T_t = \mathrm{Id}$ on $\Gamma_D \cup \Gamma_N \cup \Gamma$. In view of (39), taking $\boldsymbol{v}_t = \boldsymbol{v} \circ T_t^{-1}$ for any $\boldsymbol{v} \in \mathbf{V}$ in (40), we can have

$$\int_\Omega A_\Omega : \mathcal{E}\left(t, \boldsymbol{u}^t\right) : \mathscr{E}(t, \boldsymbol{u}^t, \boldsymbol{v})\xi(t)\mathrm{d}x =$$
$$= \int_\Omega (\boldsymbol{f} \circ T_t) \cdot \boldsymbol{v}\xi(t)\mathrm{d}x + \int_{\Gamma_N} (\boldsymbol{g} \circ T_t) \cdot \boldsymbol{v}\xi(t)|\mathrm{D}T_t^{-T}\boldsymbol{n}|\mathrm{d}s \quad \forall \boldsymbol{v} \in \mathbf{V}. \tag{41}$$

For the shape functional,

$$J\left(\Omega_t\right) = \int_{\Omega_t} j(\boldsymbol{u}_t)\mathrm{d}x_t + \int_{\Gamma_N} l(\boldsymbol{u}_t)\mathrm{d}s_t$$
$$= \int_\Omega j(t, \boldsymbol{u}^t)\xi(t)\mathrm{d}x + \int_{\Gamma_N} l(t, \boldsymbol{u}^t)\xi(t)|\mathrm{D}T_t^{-T}\boldsymbol{n}|\mathrm{d}s, \tag{42}$$

where we denote $j(t, \boldsymbol{u}^t) := j(\boldsymbol{u}_t \circ T_t)$ and $l(t, \boldsymbol{u}^t) := l(\boldsymbol{u}_t \circ T_t)$. Introduce a Lagrangian

$$L(t, \boldsymbol{\varphi}, \boldsymbol{\psi})$$
$$:= \int_\Omega j(t, \boldsymbol{\varphi})\xi(t)\mathrm{d}x + \int_{\Gamma_N} l(t, \boldsymbol{\varphi})\xi(t)|\mathrm{D}T_t^{-T}\boldsymbol{n}|\mathrm{d}s + \int_\Omega A_\Omega \mathcal{E}(t, \boldsymbol{\varphi}) : \mathscr{E}(t, \boldsymbol{\varphi}, \boldsymbol{\psi})\xi(t)\mathrm{d}x$$
$$- \int_\Omega (\boldsymbol{f} \circ T_t) \cdot \boldsymbol{\psi}\xi(t)\mathrm{d}x - \int_{\Gamma_N} (\boldsymbol{g} \circ T_t) \cdot \boldsymbol{\psi}\xi(t)|\mathrm{D}T_t^{-T}\boldsymbol{n}|\mathrm{d}s. \tag{43}$$

In view of (3) and (42), we have $J\left(\Omega_t\right) = L\left(t, \boldsymbol{u}^t, \boldsymbol{\psi}\right)$ for all $\boldsymbol{\psi} \in \mathbf{V}$. Thus, the shape derivative can be computed as

$$dJ(\Omega; \boldsymbol{\theta}) = \left. \frac{\mathrm{d}}{\mathrm{d}t} L\left(t, \boldsymbol{u}^t, \boldsymbol{\psi}\right) \right|_{t=0}. \tag{44}$$

The advantage of the Lagrangian is that, under suitable assumptions, one can show that

$$\left. \frac{\mathrm{d}}{\mathrm{d}t} L\left(t, \boldsymbol{u}^t, \boldsymbol{\psi}\right) \right|_{t=0} = \partial_t L\left(0, \boldsymbol{u}^0, \boldsymbol{p}^0\right), \tag{45}$$

which essentially means that it is unnecessary to compute the derivative of $\boldsymbol{u}^t$ in order to calculate $dJ(\Omega; \boldsymbol{\theta})$. Using (44) and (45), we obtain (30).

To derive the boundary form of the Eulerian derivative, consider a Lagrangian

$$\mathcal{L}(\Omega, \boldsymbol{u}, \boldsymbol{p}) = \int_{\Omega} j(\boldsymbol{u}) \, \mathrm{d}x + \int_{\Omega} A : E(\boldsymbol{u}) : \hat{E}(\boldsymbol{u}, \boldsymbol{p}) \, \mathrm{d}x - \int_{\Omega} \boldsymbol{f} \cdot \boldsymbol{p} \, \mathrm{d}x$$
$$- \int_{\Gamma_N} \boldsymbol{g} \cdot \boldsymbol{p} \, \mathrm{d}s + \ell \mathrm{Vol}(\Omega). \tag{46}$$

We have

$$dJ(\Omega; \boldsymbol{\theta}) = \int_{\partial\Omega} (j(\boldsymbol{u}) + A : E(\boldsymbol{u}) : \hat{E}(\boldsymbol{u}, \boldsymbol{p}) - \boldsymbol{f} \cdot \boldsymbol{p} + \ell) \theta_n \, \mathrm{d}s$$
$$- \int_{\Gamma_N} \left(\frac{\partial (\boldsymbol{g} \cdot \boldsymbol{p})}{\partial \boldsymbol{n}} + \kappa(g \cdot \boldsymbol{p}) \right) \theta_n \, \mathrm{d}s, \tag{47}$$

where κ is the mean curvature. Since the boundaries Γ_N and Γ_D are not deformed, we obtain the boundary expression (35). ∎

For a compliant mechanism of linear elasticity, we can obtain from Laurain (2018, Section 3) the distributed Eulerian derivative

$$dJ(\Omega; \boldsymbol{\theta}) = - \int_{\Omega} \mathrm{D}\boldsymbol{u}^T \mathcal{S}(A\boldsymbol{\varepsilon}(\boldsymbol{p})) : \mathrm{D}\boldsymbol{\theta} \, \mathrm{d}x - \int_{\Omega} \mathrm{D}\boldsymbol{p}^T \mathcal{S}(A\boldsymbol{\varepsilon}(\boldsymbol{u})) : \mathrm{D}\boldsymbol{\theta} \, \mathrm{d}x$$
$$+ \int_{\Omega} A\boldsymbol{\varepsilon}(\boldsymbol{u}) : \boldsymbol{\varepsilon}(\boldsymbol{p}) \, \mathrm{div} \, \boldsymbol{\theta} \, \mathrm{d}x, \tag{48}$$

where $\boldsymbol{u}$ satisfies (4) and $\boldsymbol{p}$ satisfies:

$$\int_{\Omega} A\boldsymbol{\varepsilon}(\boldsymbol{p}) : \boldsymbol{\varepsilon}(\boldsymbol{\psi}) \mathrm{d}x + \int_{\Gamma_{out}} k_s \boldsymbol{p} \cdot \boldsymbol{\psi} \mathrm{d}s = -\eta_{\mathrm{in}} \int_{\Gamma_{\mathrm{in}}} \psi_1 \mathrm{d}s - \eta_{\mathrm{out}} \int_{\Gamma_{\mathrm{out}}} \psi_1 \mathrm{d}s$$
$$\forall \boldsymbol{\psi} \in \mathbf{V} \tag{49}$$

with $\boldsymbol{\psi} = (\psi_1, \psi_2)$.

For the sake of simplicity, the nonlinear elastic structure is used with a single input and a single output. The derivation for the distributed Eulerian derivative of the compliant mechanism of (5) is similar to that of Theorem 3.2. We omit proof for simplicity to obtain the following result.

THEOREM 3.3 (COMPLIANT MECHANISM IN NONLINEAR ELASTICITY) *Let Ω be an open bounded domain. Let $\boldsymbol{u}$ be the solution to state (18) and $\boldsymbol{p}$ satisfy the adjoint problem:*

$$\int_{\Omega} A : \delta \tilde{E}(\boldsymbol{u}, \boldsymbol{\psi}) : \hat{E}(\boldsymbol{u}, \boldsymbol{p}) \mathrm{d}x + \int_{\Omega} A : E(\boldsymbol{u}) : \delta \bar{E}(\boldsymbol{u}, \boldsymbol{p}, \boldsymbol{\psi}) \mathrm{d}x + \int_{\Gamma_{out}} k_s \boldsymbol{p} \cdot \boldsymbol{\psi} \, \mathrm{d}s$$

$$= -\eta_{\text{in}} \int_{\Gamma_{\text{in}}} \psi_1 \mathrm{d}s - \eta_{\text{out}} \int_{\Gamma_{\text{out}}} \psi_1 \mathrm{d}s \ \forall \boldsymbol{\psi} \in \mathbf{V}. \tag{50}$$

Then, the volume expression of the Eulerian derivative of (5) *reads:*

$$
\begin{aligned}
dJ(\Omega; \boldsymbol{\theta}) = \int_{\Omega} \Big(A\partial_t \mathcal{E}(0, \boldsymbol{u}) : \mathscr{E}(0, \boldsymbol{u}, \boldsymbol{p}) \mathcal{E}(0, \boldsymbol{u}) : \partial_t \mathscr{E}(0, \boldsymbol{u}, \boldsymbol{p}) \\
+ A\mathcal{E}(0, \boldsymbol{u}) : \mathscr{E}(0, \boldsymbol{u}, \boldsymbol{p}) \operatorname{div} \boldsymbol{\theta} \Big) \mathrm{d}x,
\end{aligned}
\tag{51}
$$

where $\partial_t \mathcal{E}(0, \boldsymbol{u})$, $\partial_t \mathscr{E}(0, \boldsymbol{u}, \boldsymbol{p})$, $\mathcal{E}(0, \boldsymbol{u})$, *and* $\mathscr{E}(0, \boldsymbol{u}, \boldsymbol{p})$ *are defined in* (31), (32), (33), *and* (34), *respectively.*

4.   Discontinuous Galerkin method

To introduce the DGFEM, we first introduce notations for the spatial discretization (Arnold et al., 2002; Hansbo and Larson, 2022; Rivière et al, 2003). For Ω, we have non-degenerate quasi-uniform meshes $\mathcal{T} = \{T_1, T_2, ..., T_{N_h}\}$, where T_j $(j = 1, \cdots, N_h)$ is a mesh element. The set of edges, denoted by E, in the mesh is divided into four subsets:

$$E = E_I \cup E_D \cup E_N \cup E_0,$$

where E_I is the set of faces in the interior of Ω, E_D and E_N are the sets of faces associated with the Dirichlet and inhomogeneous Neumann boundary conditions, respectively, and E_0 corresponds to the homogeneous Neumann boundary.

Let $L^2(\Omega)$ be the space of Lebesgue square-integrable functions. Denote $\boldsymbol{L}^2(\Omega) := L^2(\Omega)^d$. We then define the following spaces:

$$D^s(\mathcal{T}) = \left\{ v \in L^2(\Omega) : v|_{T_j} \in H^{s+\iota}(T_j) \forall T_j \in \mathcal{T}, j = 1, ..., N_h \text{ and some } \iota > 0 \right\},$$
$$\boldsymbol{D}^s(\mathcal{T}) = \left\{ \boldsymbol{v} \in \boldsymbol{L}^2(\Omega) : v_i \in D^s(\mathcal{T}), i = 1, \cdots, d \right\},$$
$$\boldsymbol{DP}_r(\mathcal{T}) = \left\{ \boldsymbol{v} : v_i|_{T_j} \in \mathbb{P}^r(T_j), \forall i = 1, \cdots, d; j = 1, \cdots, N_h \right\},$$
$$\boldsymbol{P}_r(\mathcal{T}) = \left\{ \boldsymbol{v} : v_i \in C^0(\overline{\Omega}), v_i|_{T_j} \in \mathbb{P}^r(T_j), \forall i = 1, \cdots, d; j = 1, \cdots, N_h \right\},$$

where $\mathbb{P}^r$ means the set of polynomials of degree less than or equal to $r \in \mathbb{N}$. For any function $\boldsymbol{v} \in \boldsymbol{D}^s(\mathcal{T})$ on the face e when $s \geq \frac{1}{2}$, we define the average and the jump for $\boldsymbol{v}$ as:

$$
\langle \boldsymbol{v} \rangle =
\begin{cases}
\boldsymbol{v}^+ & e \in E_D \text{ or } e \in E_N, \\
\dfrac{1}{2}\boldsymbol{v}^+ + \dfrac{1}{2}\boldsymbol{v}^- & e \in E_I,
\end{cases}
\tag{52}
$$

$$\llbracket \boldsymbol{v} \rrbracket = \begin{cases} \boldsymbol{v}^+ & e \in E_D \text{ or } e \in E_N, \\ \boldsymbol{v}^+ - \boldsymbol{v}^- & e \in E_I, \end{cases} \tag{53}$$

where

$$\boldsymbol{v}^\mp = \lim_{\epsilon \to 0^+} \boldsymbol{v}(\boldsymbol{x} \pm \epsilon \boldsymbol{n}_e), \quad \forall \boldsymbol{x} \in e$$

with $\boldsymbol{n}_e$ being the exterior unit normal on each face.

Linear elasticity (Rivière et al., 2003). Consider a penalized weak form of the linear elasticity problem (1): find $\boldsymbol{u} \in \boldsymbol{D}^{\frac{3}{2}}(T)$ such that

$$a(\boldsymbol{u}, \boldsymbol{v}) + J(\boldsymbol{u}, \boldsymbol{v}) = l(\boldsymbol{v}) \quad \forall \boldsymbol{v} \in \boldsymbol{D}^{\frac{3}{2}}(\mathcal{T}), \tag{54}$$

where

$$a(\boldsymbol{u}, \boldsymbol{v}) = \sum_{T_i \in \mathcal{T}} \int_{T_i} \boldsymbol{\sigma}(\boldsymbol{u}) : \boldsymbol{\varepsilon}(\boldsymbol{v}) \mathrm{d}x - \sum_{e \in E_D} \int_e \langle \boldsymbol{n} \cdot \boldsymbol{\sigma}(\boldsymbol{u}) \rangle : \llbracket \boldsymbol{v} \rrbracket \mathrm{d}s$$

$$- \sum_{e \in E_I} \int_e \langle \boldsymbol{n} \cdot \sigma(\boldsymbol{u}) \rangle : \llbracket \boldsymbol{v} \rrbracket \mathrm{d}s$$

$$+ \sum_{e \in E_D} \int_e \langle \boldsymbol{n} \cdot \boldsymbol{\sigma}(\boldsymbol{v}) \rangle : \llbracket \boldsymbol{u} \rrbracket \mathrm{d}s + \sum_{e \in E_I} \int_e \langle \boldsymbol{n} \cdot \boldsymbol{\sigma}(\boldsymbol{v}) \rangle : \llbracket \boldsymbol{u} \rrbracket \mathrm{d}s,$$

$$J(\boldsymbol{u}, \boldsymbol{v}) = \sum_{e \in E_D} \int_e \frac{\gamma_0}{|e|} \llbracket \boldsymbol{u} \rrbracket \cdot \llbracket \boldsymbol{v} \rrbracket \mathrm{d}s + \sum_{e \in E_I} \int_e \frac{\gamma_0}{|e|} \llbracket \boldsymbol{u} \rrbracket \cdot \llbracket \boldsymbol{v} \rrbracket \mathrm{d}s,$$

$$l(\boldsymbol{v}) = \int_\Omega \boldsymbol{f} \cdot \boldsymbol{v} \mathrm{d}x + \int_{\Gamma_N} \boldsymbol{g} \cdot \boldsymbol{v} \mathrm{d}s,$$

with $\gamma_0 > 0$ being a penalty parameter and $|e|$ being the measure of e.

A finite-dimensional discontinuous Galerkin weak formulation, associated with (54), reads: find $\boldsymbol{u}_{\mathrm{DG}} \in \boldsymbol{DP}_r(\mathcal{T})$ such that

$$a(\boldsymbol{u}_{\mathrm{DG}}, \boldsymbol{v}) + J(\boldsymbol{u}_{\mathrm{DG}}, \boldsymbol{v}) = l(\boldsymbol{v}) \quad \forall \boldsymbol{v} \in \boldsymbol{DP}_r(\mathcal{T}). \tag{55}$$

Nonlinear elasticity (Hansbo and Larson, 2022). We use the Newton method (Kim, 2015) to solve (16) by updating

$$\boldsymbol{u}^{k+1} = \boldsymbol{u}^k + \Delta \boldsymbol{u}^k, \tag{56}$$

where the incremental $\Delta \boldsymbol{u}^k \in \boldsymbol{P}_r(T)$ satisfies the following:

$$a^*(\boldsymbol{u}^k; \Delta \boldsymbol{u}^k, \boldsymbol{\psi}) = l(\boldsymbol{\psi}) - a(\boldsymbol{u}^k, \boldsymbol{\psi}) \quad \forall \boldsymbol{\psi} \in \boldsymbol{P}_r(T), \tag{57}$$

in which

$$a^*(\boldsymbol{u}^k; \Delta\boldsymbol{u}^k, \boldsymbol{\psi}) =$$
$$= \int_\Omega \Big[A : \hat{E}(\boldsymbol{u}^k, \boldsymbol{\psi}) : \Delta E(\boldsymbol{u}^k, \Delta\boldsymbol{u}^k) + A : E(\boldsymbol{u}^k) : \Delta\hat{E}(\Delta\boldsymbol{u}^k, \boldsymbol{\psi}) \Big] \mathrm{d}x,$$

with

$$\hat{E}(\boldsymbol{u}^k, \boldsymbol{\psi}) = \mathcal{S}((I + \mathrm{D}\boldsymbol{u}^k)^T \cdot \mathrm{D}\boldsymbol{\psi}),$$
$$\Delta E(\boldsymbol{u}^k, \Delta\boldsymbol{u}^k) = \mathcal{S}((I + \mathrm{D}\boldsymbol{u}^k)^T \cdot \mathrm{D}\Delta\boldsymbol{u}^k),$$
$$\Delta\hat{E}(\Delta\boldsymbol{u}^k, \boldsymbol{\psi}) = \mathcal{S}(\mathrm{D}\boldsymbol{\psi}^T \cdot \mathrm{D}\Delta\boldsymbol{u}^k).$$

We now use the discontinuous Galerkin method to solve the nonlinear elasticity problem. Define a mesh function h by

$$h|_e = \min\left\{ \frac{|T^+|}{|e|}, \frac{|T^-|}{|e|} \right\} \quad \text{for } e = \partial T^+ \cap \partial T^-. \tag{58}$$

Thus, the discontinuous Galerkin Newton iteration scheme reads (Hansbo and Larson, 2022):

$$\boldsymbol{u}^{k+1} = \boldsymbol{u}^k + \Delta\boldsymbol{u}^k, \tag{59}$$

in which $\Delta\boldsymbol{u}^k \in \boldsymbol{DP}_r(T)$ satisfies

$$b^*(\Delta\boldsymbol{u}^k, \boldsymbol{\psi}) = l(\boldsymbol{\psi}) - b(\boldsymbol{u}^k, \boldsymbol{\psi}) \quad \forall\boldsymbol{\psi} \in \boldsymbol{DP}_r(T), \tag{60}$$

where

$$
\begin{aligned}
b(\boldsymbol{u}^k, \boldsymbol{\psi}) = &\sum_{T_i \in T} \int_{T_i} A : E(\boldsymbol{u}^k) : \hat{E}(\boldsymbol{u}^k, \boldsymbol{\psi}) \mathrm{d}x \\
&- \sum_{e \in E_D \cup E_I} \int_e A : E(\langle\boldsymbol{u}^k\rangle) : \widetilde{E}(\langle\boldsymbol{u}^k\rangle, [\![\boldsymbol{\psi}]\!]) \mathrm{d}s \\
&+ \sum_{e \in E_D \cup E_I} \int_e \frac{\gamma_0}{h} A : \widetilde{E}(\langle\boldsymbol{u}^k\rangle, [\![\boldsymbol{u}^k]\!]) : \widetilde{E}(\langle\boldsymbol{u}^k\rangle, [\![\boldsymbol{\psi}]\!]) \mathrm{d}s \\
&+ \sum_{e \in E_D \cup E_I} \int_e \frac{\gamma_0}{h} A : E(\langle\boldsymbol{u}^k\rangle) : \Delta\widetilde{E}([\![\boldsymbol{\psi}]\!], [\![\boldsymbol{u}^k]\!]) \mathrm{d}s \\
&- \sum_{e \in E_D \cup E_I} \int_e A : \widetilde{E}(\langle\boldsymbol{u}^k\rangle, [\![\boldsymbol{u}^k]\!]) : \Delta E(\langle\boldsymbol{u}^k\rangle, \langle\boldsymbol{\psi}\rangle) \mathrm{d}s \\
&- \sum_{e \in E_D \cup E_I} \int_e A : E(\langle\boldsymbol{u}^k\rangle) : \Delta\check{E}(\langle\boldsymbol{\psi}\rangle, [\![\boldsymbol{u}^k]\!]) \mathrm{d}s
\end{aligned}
$$

and

$$b^*(\Delta\boldsymbol{u}^k, \boldsymbol{\psi}) = \sum_{T_i \in T} \int_{T_i} [A : \hat{E}(\boldsymbol{u}^k, \boldsymbol{\psi}) : \Delta E(\boldsymbol{u}^k, \Delta\boldsymbol{u}^k) + A : E(\boldsymbol{u}^k) : \Delta\hat{E}(\Delta\boldsymbol{u}^k, \boldsymbol{\psi})]\mathrm{d}x$$

$$- \sum_{e \in E_D \cup E_I} \int_e A : \widetilde{E}(\langle\boldsymbol{u}^k\rangle, [\![\boldsymbol{\psi}]\!]) : \Delta E(\langle\boldsymbol{u}^k\rangle, \langle\Delta\boldsymbol{u}^k\rangle)\mathrm{d}s$$

$$- \sum_{e \in E_D \cup E_I} \int_e A : E(\langle\boldsymbol{u}^k\rangle) : \Delta\check{E}(\langle\Delta\boldsymbol{u}^k\rangle, [\![\boldsymbol{\psi}]\!])\mathrm{d}s$$

$$- \sum_{e \in E_D \cup E_I} \int_e A : \widetilde{E}(\langle\boldsymbol{u}^k\rangle, [\![\Delta\boldsymbol{u}^k]\!]) : \Delta E(\langle\boldsymbol{u}^k\rangle, \langle\boldsymbol{\psi}\rangle)\mathrm{d}s$$

$$- \sum_{e \in E_D \cup E_I} \int_e A : E(\langle\boldsymbol{u}^k\rangle) : \Delta\check{E}(\langle\boldsymbol{\psi}\rangle, [\![\Delta\boldsymbol{u}^k]\!])\mathrm{d}s$$

$$+ \sum_{e \in E_D \cup E_I} \int_e \frac{\gamma_0}{h} A : \widetilde{E}(\langle\boldsymbol{u}^k\rangle, [\![\boldsymbol{\psi}]\!]) : \widetilde{E}(\langle\boldsymbol{u}^k\rangle, [\![\Delta\boldsymbol{u}^k]\!])\mathrm{d}s$$

$$+ \sum_{e \in E_D \cup E_I} \int_e \frac{\gamma_0}{h} A : E(\langle\boldsymbol{u}^k\rangle) : \Delta\widetilde{E}([\![\Delta\boldsymbol{u}^k]\!], [\![\boldsymbol{\psi}]\!])\mathrm{d}s,$$

with

$$\widetilde{E}(\boldsymbol{u}, \boldsymbol{v}) = \mathcal{S}((I + \mathrm{D}\boldsymbol{u})^T \cdot (\boldsymbol{v} \otimes \boldsymbol{n})),$$

$$\Delta\widetilde{E}(\boldsymbol{u}, \boldsymbol{v}) = \mathcal{S}((\boldsymbol{u} \otimes \boldsymbol{n})^T \cdot (\boldsymbol{v} \otimes \boldsymbol{n})),$$

$$\Delta\check{E}(\boldsymbol{u}, \boldsymbol{v}) = \mathcal{S}((\mathrm{D}\boldsymbol{u})^T \cdot (\boldsymbol{v} \otimes \boldsymbol{n})).$$

5.   Level set method

The level set method (Osher and Sethian, 1988), as a general implicit interface-tracking technique for computation of evolving interfaces using an implicit representation of these interfaces, has been successfully applied in shape and topology optimization (see, e.g., Allaire et al., 2005; Allaire, Jouve and Toader, 2004; Fulmanski et al., 2008). The method represents the boundary of the moving domain $\Omega_t \subset D \subset \mathbb{R}^d$ as the zero level set of a continuous function $\phi(t, \cdot) : D \to \mathbb{R}$. Each domain Ω_t can be represented as

$$\Omega_t := \{\boldsymbol{x} \in D | \phi(t, \boldsymbol{x}) < 0\},$$

where $\phi : \mathbb{R}^+ \times D \to \mathbb{R}$ is a Lipschitz continuous level set function. The boundary $\partial\Omega_t$ can be the zero level set of $\phi(t, \cdot)$:

$$\partial\Omega_t = \{\boldsymbol{x} \in D | \phi(t, \boldsymbol{x}) = 0\}.$$

Let $\boldsymbol{x}(t)$ be the position of a moving boundary point of $\partial\Omega_t$, with velocity $\dot{\boldsymbol{x}}(t) = \boldsymbol{\theta}(\boldsymbol{x}(t))$. Differentiation of the relation $\phi(\boldsymbol{x}(t), t) = 0$ with respect to t yields

$$\phi_t(t, \boldsymbol{x}(t)) + \boldsymbol{\theta}(\boldsymbol{x}(t)) \cdot \nabla\phi(t, \boldsymbol{x}(t)) = 0 \ \text{ in } \mathbb{R}^+ \times \partial\Omega_t,$$

which is then extended to $\mathcal{D}$ to obtain a transport equation

$$\phi_t(t, \boldsymbol{x}) + \boldsymbol{\theta}(\boldsymbol{x}) \cdot \nabla\phi(t, \boldsymbol{x}) = 0 \ \text{ in } \mathbb{R}^+ \times D. \tag{61}$$

Rewrite (61) as $\mathcal{A}\phi(t, \boldsymbol{x}) = 0$, where

$$\mathcal{A}\phi = \phi_t(t, \boldsymbol{x}) + \boldsymbol{\theta}(t, \boldsymbol{x}) \cdot \nabla\phi(t, \boldsymbol{x}).$$

We use DGFEM for spatial discretizations of the transport equation of the level set function (see Tan and Zhu, 2023). Consider a two-dimensional case for simplicity. Let $\{\mathcal{I}_h\}_{h>0}$ be a family of triangular meshes of D. Denote by P_{1dc} the space of piecewise linear break element polynomials. Define

$$W = \{v \in L^2(D) \,|\, \boldsymbol{\theta} \cdot \nabla v \in L^2(D)\},$$
$$W_h = \{v_h \in L^2(D) \,|\, \forall K \in \mathcal{I}_h, v_h|_K \in \mathbb{P}^1(K)\}.$$

Let $W(h) = H^1(D) + W_h$. To enforce boundary conditions, define

$$\partial D^{\pm} = \{\boldsymbol{x} \in \partial D| \pm \boldsymbol{\theta}(\boldsymbol{x}) \cdot \boldsymbol{n}(\boldsymbol{x}) > 0\} \tag{62}$$

and assume that ∂D^- and ∂D^+ are well-separated.

Denote by $\mathcal{F}_h$ the set of interior faces, i.e., $F \in \mathcal{F}_h$ if F is a 1-manifold and there are $K_1(F)$, $K_2(F) \in \mathcal{I}_h$ such that $F = K_1(F) \cap K_2(F)$. Moreover, denote by $\mathcal{F}_h^\partial$ the set of the faces that separate the mesh from the exterior of D, i.e., $F \in \mathcal{F}_h^\partial$ if F is a 1-manifold and there is $K(F) \in \mathcal{I}_h$ such that $F = K(F) \cap \partial D$. Finally, we set $\mathcal{F}_h = \mathcal{F}_h \cup \mathcal{F}_h^\partial$.

We introduce $\mathscr{D}$ and $\mathscr{M} : \partial D \to \mathbb{R}$, which has the following representation: for all functions $v, w \in W$

$$\begin{aligned}
\langle \mathscr{D}v, w \rangle_{W',W} &= \int_{\partial D} vw(\boldsymbol{\theta} \cdot \boldsymbol{n}) \mathrm{d}s \\
\langle \mathscr{M}v, w \rangle_{W',W} &= \int_{\partial D} vw|\boldsymbol{\theta} \cdot \boldsymbol{n}| \mathrm{d}s.
\end{aligned} \tag{63}$$

For any measurable subset of D, let $(\cdot, \cdot)_{L,E}$ denote the usual L^2 scalar product on E. Thus, we define the bilinear form

$$\tilde{a}(\phi, w) = (\mathcal{A}\phi, w)_L + \frac{1}{2} \langle (\mathscr{M} - \mathscr{D})\phi, w \rangle_{W',W}. \tag{64}$$

To control the jumps of functions in W_h across mesh interfaces, we introduce for all $F \in \mathcal{F}_h$ a linear operator $S_F \in \mathcal{L}(L^2(F); L^2(F))$

$$S_F = \alpha |\boldsymbol{\theta} \cdot \boldsymbol{n}_F|, \tag{65}$$

where $\boldsymbol{n}_F$ is a unit vector normal to F. Since every function v in W_h has a (possibly two-valued) trace almost everywhere on $F \in \mathcal{F}_h$, it means that for a.e. $\boldsymbol{x} \in F$,

$$v^1(\boldsymbol{x}) = \lim_{\substack{\boldsymbol{y} \to \boldsymbol{x} \\ \boldsymbol{y} \in K_1(F)}} v(\boldsymbol{y}), \;\; v^2(\boldsymbol{x}) = \lim_{\substack{\boldsymbol{y} \to \boldsymbol{x} \\ \boldsymbol{y} \in K_2(F)}} v(\boldsymbol{y}). \tag{66}$$

Thus, we define on F

$$[\![v]\!] = v^1 - v^2, \quad \{v\} = \frac{1}{2}(v^1 + v^2).$$

We introduce the bilinear form $\tilde{a}_h$ such that for all ϕ, w in $W(h)$,

$$\begin{aligned}
\tilde{a}_h(\phi, w) = &\sum_{K \in \mathcal{I}_h} (\mathcal{A}\phi, w)_{L,K} + \sum_{K \in \mathcal{F}_h^\partial} \frac{1}{2}(\mathcal{M}(\phi) - \mathcal{D}\phi, w)_{L,F} \\
&- \sum_{K \in \mathcal{F}_h} 2(\{\mathcal{D}\phi\}, \{w\})_{L,F} + \sum_{F \in \mathcal{F}_h} (S_F([\![\phi]\!]), [\![w]\!])_{L,F}.
\end{aligned} \tag{67}$$

The flux of a function v on ∂K, say $\zeta_{\partial K}(v) \in L^2(\partial K)$, is defined on a face $F \subset \partial K$ by

$$\zeta_{\partial K}(v)|_F = \begin{cases} \frac{1}{2}\mathcal{M}(v|_F) - \frac{1}{2}\mathcal{D}v & \text{if } F \in \mathcal{F}^\partial \\ S_F([\![v]\!]_{\partial K}|_F) - \mathcal{D}\{v\}_{\partial K} & \text{if } F \in \mathcal{F}. \end{cases}$$

Then we have the discretized variational formulation: Find $\phi_h \in W_h$ such that $\forall K \in \mathcal{I}_h$ and $w_h \in W_h$

$$(\mathcal{A}\phi_h, w_h)_{L,K} + (\zeta_{\partial K}(\phi_h), w_h)_{L,\partial K} = 0.$$

Here, the interface/boundary flux of the level-set transport equation is

$$\zeta_{\partial K}(\phi_h)|_F, = \begin{cases} (\alpha|\boldsymbol{\theta} \cdot \boldsymbol{n}_K| - \frac{1}{2}\boldsymbol{\theta} \cdot \boldsymbol{n}_K)[\![\phi_h]\!]_{\partial K} & \text{if } F \in \mathcal{F}^\partial \\ -|\boldsymbol{\theta} \cdot \boldsymbol{n}|\phi_h \mathbf{1}_{\partial D^-} & \text{if } F \in \mathcal{F}, \end{cases}$$

where $\mathbf{1}_{\partial D^-}$ denotes the characteristic function of ∂D^-. We now consider time discretization using the backward Euler method. Denote by $\delta t > 0$ the time step. Let ϕ_h^n be an approximation to $\phi^n = \phi(t_n, \boldsymbol{x})$ at $t_n = n\delta t$. The space-time

discretization of (68) reads: Given ϕ_h^n $(n = 0, 1, \cdots)$, find $\phi_h^{n+1} \in W_h$ such that $\forall w \in W_h$

$$\int_D \left(\frac{\phi_h^{n+1} - \phi_h^n}{\delta t} + \boldsymbol{\theta} \cdot \nabla \phi_h^{n+1} \right) w \mathrm{d}\boldsymbol{x} + \sum_{\partial K} \int_{\partial K} \left(\alpha |\boldsymbol{n}_K \cdot \boldsymbol{\theta}| - \frac{1}{2} \boldsymbol{n}_K \cdot \boldsymbol{\theta} \right) [\![\phi_h^{n+1}]\!] w \mathrm{d}s$$

$$- \sum_{\partial K_\Gamma^-} \int_{K_\Gamma^-} |\boldsymbol{n} \cdot \boldsymbol{\theta}| \phi_h^{n+1} w \mathrm{d}s = 0, \qquad (68)$$

where ∂K is the set of inner edges, and ∂K_Γ^- is the set of boundary edges, and where $\boldsymbol{\theta} \cdot \boldsymbol{n}_K < 0$. The normal vector $\boldsymbol{n}_K$ here is the normal to the edges of each inner element.

For reinitialization of the level set function, we use an effective iteration scheme integrated into FreeFem++ as a plug-in function "distance" to complete periodical reinitialization (Dapogny and Frey, 2010).

6.   Numerical results

Numerical examples are tested with FreeFem++ (Hecht, 2012). For linear elasticity, we use the distributed Eulerian derivative for numerical computation. Considering that the complicated expression of distributed Eulerian derivatives in nonlinear elasticity causes high computational costs, we test the numerical algorithm with the boundary type of Eulerian derivative. The Lamé parameters are

$$\lambda = \frac{E}{2(1 + \nu)}, \quad \mu = \frac{\nu E}{2(1 + \nu)(1 - \nu)}$$

with E and ν being Young's modulus and Poisson's ratio of the material, respectively. We choose $E = 1$ Gpa (respectively 0.36 Gpa) and $\nu = 0.3$ (respectively 0.48) for linear elasticity (respectively nonlinear elasticity), if not specified otherwise below. We consider a unit load $\boldsymbol{g} = (0, -1)$, if not specified otherwise below. In the figures provided further on for the convergence history of the objective, the objective quantity does not contain the volume term.

6.1.   Compliance problem

EXAMPLE 1 (LINEAR ELASTICITY) *Consider four cases for linear elasticity: cantilever, bridge, T-structure, and plate structure.*

Case 1 (Cantilever): A design problem for cantilever beam is shown in Fig. 2 (upper-left). The design domain is a 2×1 rectangle with fixed boundary conditions on the left side, and a unit vertical point load at the center on the right. The domain is discretized using 45 494 triangular meshes. We set $\ell = 0.25$. Two initial designs, shown in Fig. 2 (upper-middle and lower-left), converge to different optimized configurations (upper-right and lower-right) due to the initial-dependent multi-scale structure of the model. Fig. 3 shows the two cases' convergence to the the same value of the objective but different volume fractions.

Case 2 (Bridge): As shown in Fig. 4 (left), the design domain is a 2×1 rectangle with fixed boundary conditions on the left and right bottom corners. A unit vertical point load is applied at the center of the bottom. Set $\ell = 2$. The mesh is the same as in the cantilever case. Fig. 4 (middle) and Fig. 4 (right) show the initial design and the optimized configuration, respectively.

Case 3 (T-structure): A design problem for the T-structure is shown in Fig. 5 (left). A vertical downward load is applied to the left and right ends of the "T" shape, and the bottom ends are fixed. We set $\ell = 0.2$. For triangulation, 22 694 mesh elements are used. Fig. 5 shows the design process. Fig. 6 (left) shows the convergence history of the objective.

Case 4 (Plate structure): A simple supported plate model (Kwak and Cho, 2005) is considered, as shown in Fig. 7 (upper left). The design domain is a 2×1 rectangle with fixed boundary conditions on the left and right sides and a unit vertical point load at the center on the top. The domain is discretized using 29 146 triangular mesh elements. We set $\ell = 4$. Fig. 7 shows the evolution process. See convergence history of the objective in Fig. 6 (right).

EXAMPLE 2 (NONLINEAR ELASTICITY: CANTILEVER) *For stiffness maximization of nonlinear structures, consider problem settings similar as shown in Fig. 2 (upper-left). Set $\ell = 15$. In Fig. 8, with $E = 0.36$ Gpa and $\nu = 0.48$, complex (upper-left) and simple (upper-right) initial designs converge to designs of upper-middle and down-left, respectively, which are similar as those of Case 1 of **Example 1**. See Fig. 9 for comparisons of convergence histories of the objective and volume fractions. Then we consider a Saint Venant-Kirchhoff material with $E = 1000$ Gpa and $\nu = 0.3$ (Ciarlet, 1998). Set $\boldsymbol{g} = (0, -3)$. The results in Fig. 8 (lower-middle and lower-right), as expected, show loss of symmetries due to the large load applied. This phenomenon coincides well with that in Allaire, Jouve and Toader (2004), where the nonlinear elasticity system was discretized with conventional continuous finite element method. We thus think the asymmetry is not a consequence of the use of DGFEM.*
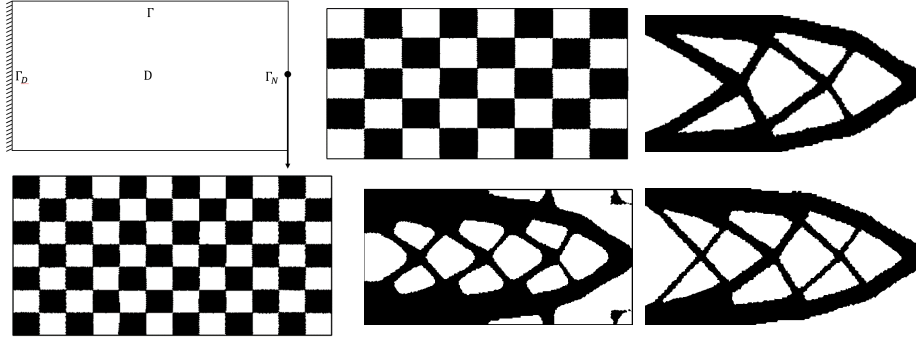
Figure 2: A design domain (upper-left), a simple initial shape (upper-middle), the final shape (upper-right), a more complicated initial shape (lower-left), design at iteration=30 (lower-middle), and the final shape (lower-right) for Case 1 of Example 1

Example 3 (Nonlinear elasticity: MBB) *As shown in Fig. 10 (left), the problem setting and mesh are the same as in Fig. 4 (left), except for the fact that the lower-right corner has a different boundary condition. Set $\ell = 10$. Fig. 10 shows the optimized design and its deformed shape. The convergence history of the objective is shown in Fig. 11.*

6.2. Compliant mechanism

The displacement inverter converts an input displacement on the left edge into a displacement in the opposite direction on the right edge as in Fig. 1. Set $D = (0,1)^2$. An actuation force $\boldsymbol{g} = (g_x, 0)$ with $g_x = 50$ is applied at the center of the left boundary. An artificial spring with stiffness $k_s = 0.1$ is attached at the output Γ_{out} to simulate the resistance of a workpiece. For triangulation, 32 282 mesh elements are used.

Example 4 (Linear elasticity) *Set $\ell = 30$. Fig. 12 shows topological changes and an optimized design with symmetry is obtained for compliant mechanism in linear elasticity. See Fig. 13 for convergence histories of the objective and volume fraction values.*

Example 5 (Nonlinear elasticity) *In Fig. 14 it is shown that for nonlinear elasticity, an asymmetric optimized design, different from the symmetric design in Fig. 12 (right) for linear elasticity, is achieved with $\ell = 35$. The*
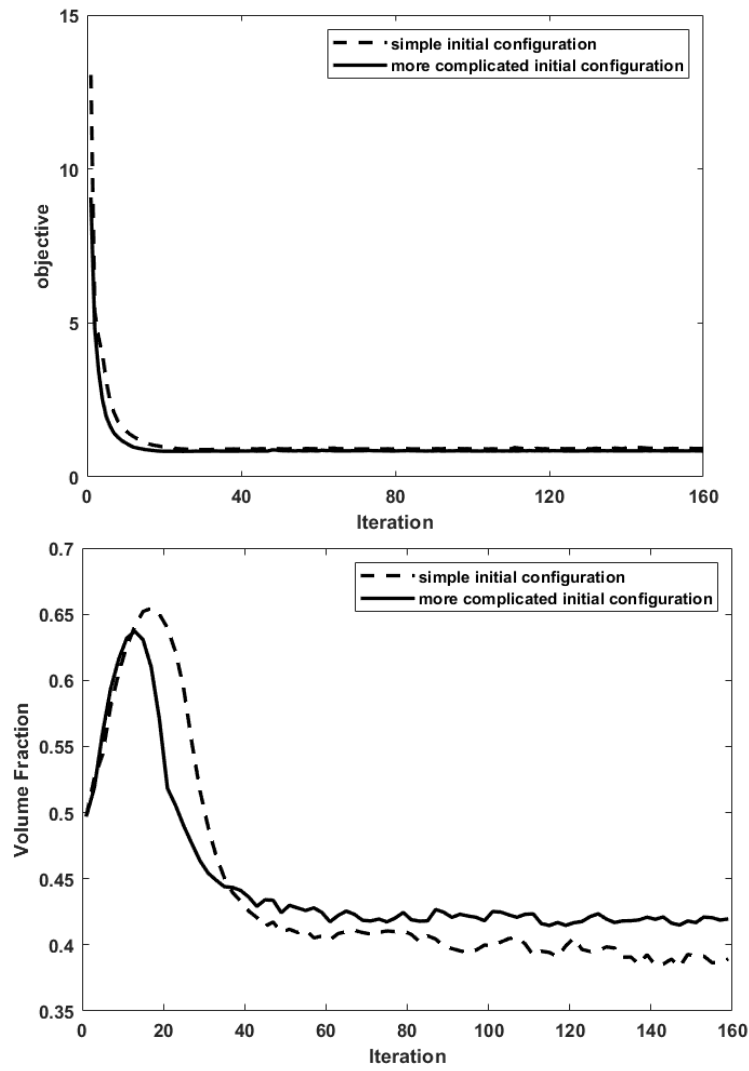
Figure 3: Convergence history of the objective (top) and volume fraction (bottom) values for Case 1 of Example 1
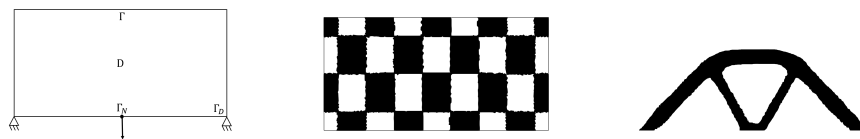
Figure 4: Problem setting, initial design, and the final shape (right) for Case 2 of Example 1
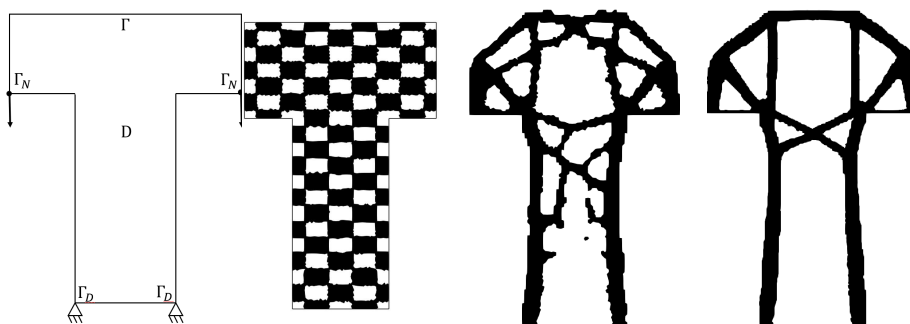
Figure 5: Problem setting, initial design, design after 20 iterations, and the final design (from left to right) for Case 3 of Example 1

convergence histories of the objective and volume fraction values are shown in Fig. 15.

Overall, topology optimization of nonlinear elasticity is more complicated than for the linear elasticity case in terms of both sensitivity analysis and programming required for numerical computation. The computational cost is also clearly higher.

Besides, DGFEM itself is more complicated and computationally more expensive than the usual (continuous) FEM in programming for both linear and nonlinear elasticity. However, the DGFEM's advantages of high-order accuracy, adaptability, and parallelism for solving complex physical systems make it worth to be studied and used for structural topology optimization.

7.   Conclusions

We have developed and implemented a level set method, based on finite element method of discontinuous Galerkin type, for structural shape and topology opti-
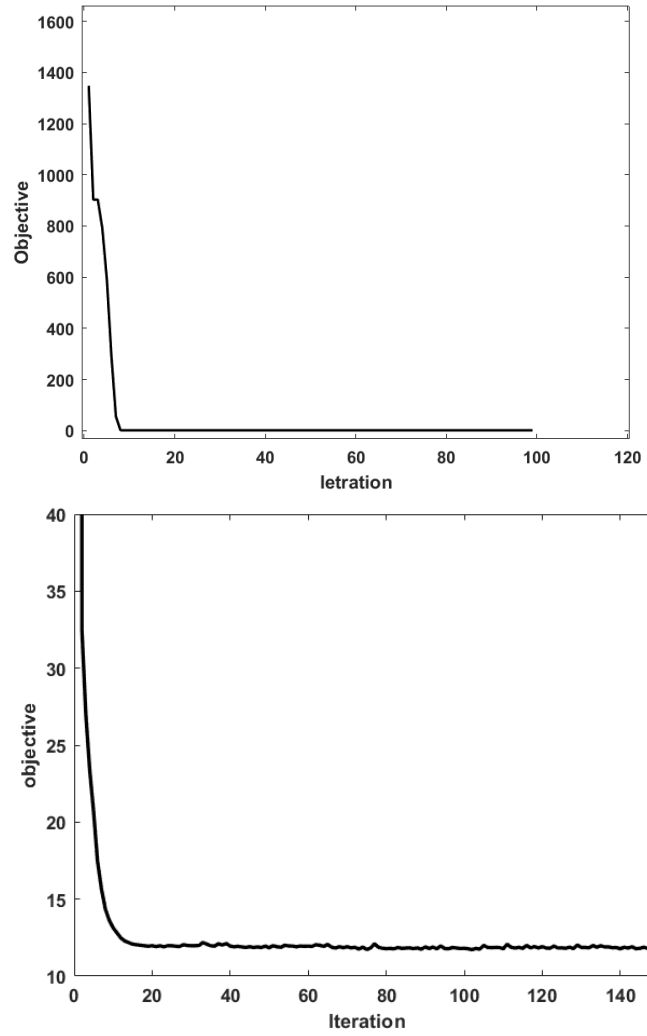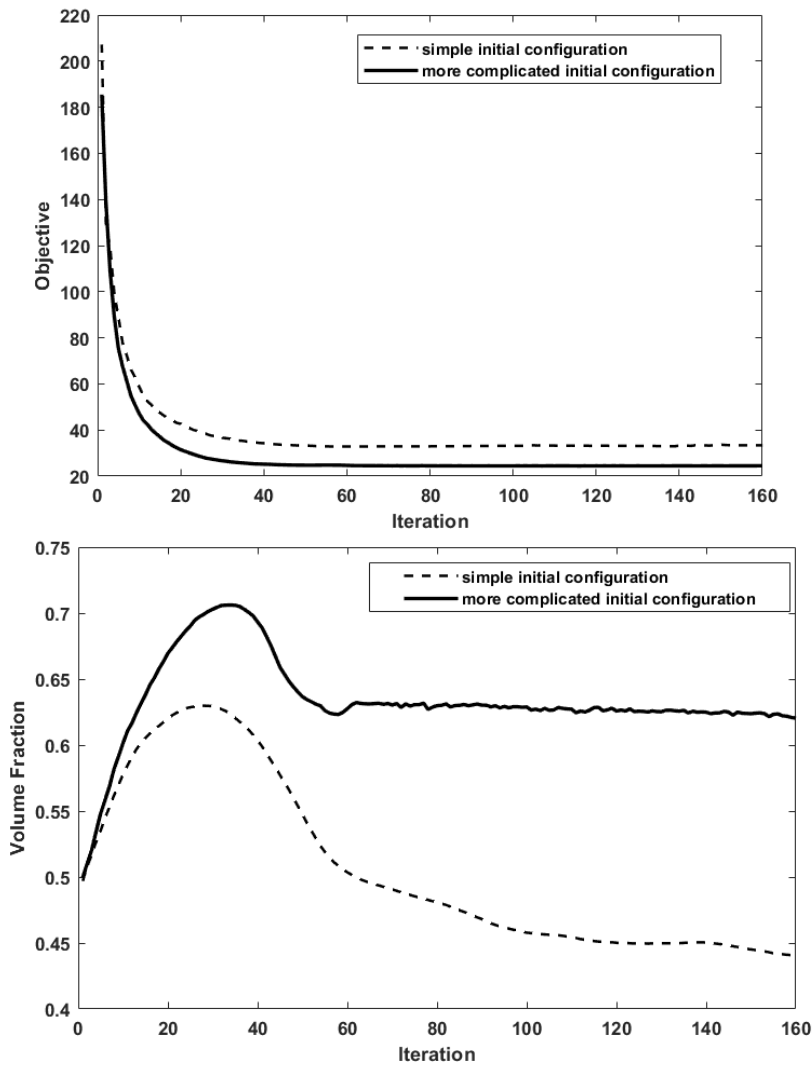
Figure 6: Convergence history of the objective: Case 3 (top) and Case 4 (bottom) of Example 1
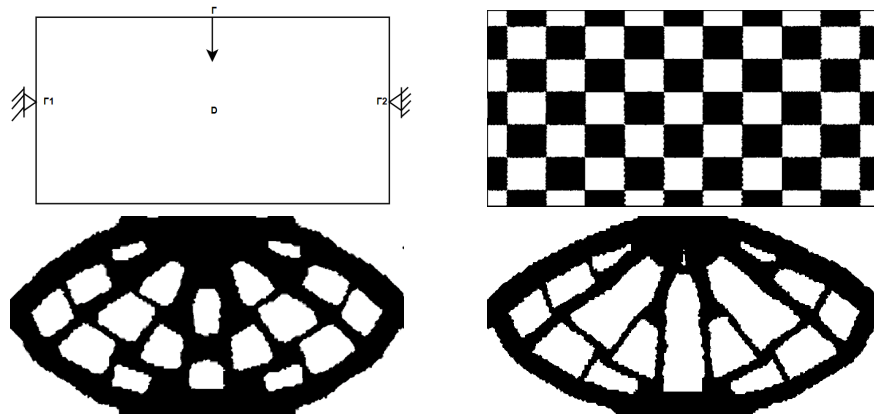
Figure 7: Design domain (upper left), initial shape (upper right), design at iteration 15 (bottom left), and final shape (bottom right) for Case 4 of Example 1
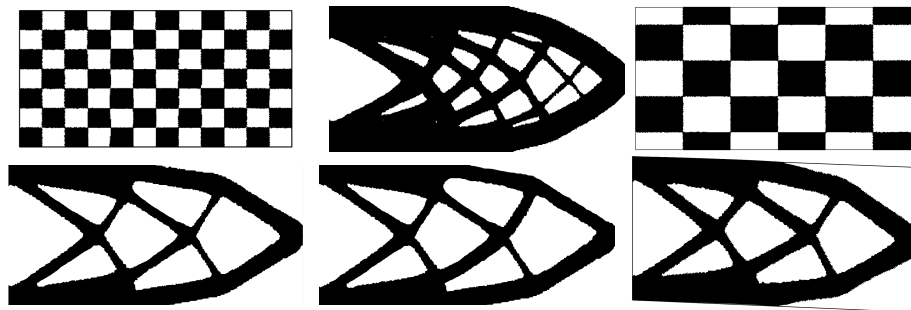
Figure 8: A complicated initial design (upper left), the final shape (upper middle), a simpler initial design (upper right), its final design with $E = 0.36$ Gpa and $\nu = 0.48$ (lower left), its final design with $E = 1000$ Gpa and $\nu = 0.3$ (lower middle), and deformed structure (lower right) for Example 2

Figure 9: Convergence history of objective (top) and volume fraction (bottom) of Example 2
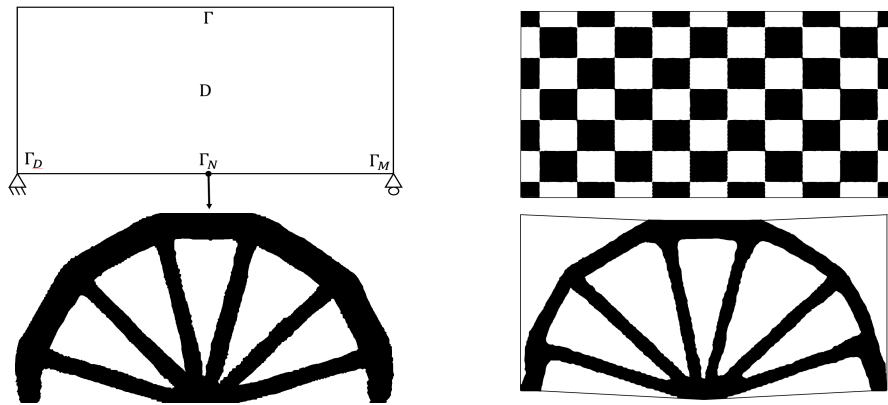
Figure 10: A design domain (upper-left), initial shape (upper-right), the final shape (lower-left) and the deformed structure (lower-right) for Example 3
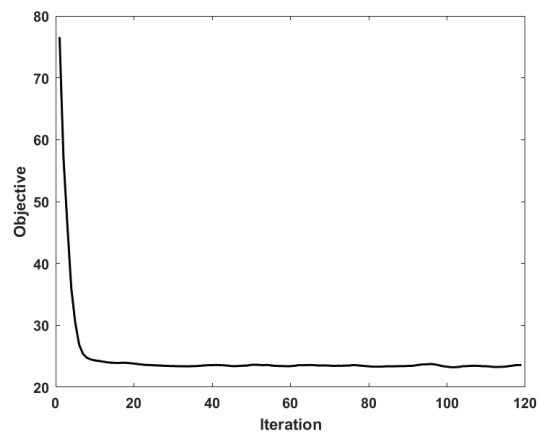
Figure 11: Convergence history of the objective values for Example 3

Figure 12: Initial design (left), design at iteration 20 (middle) and final shape (right) values for Example 4: linear elasticity

mization. DGFEM is used in both stages of analysis and design. Both stiffness and compliant designs are considered for linear and nonlinear elastic structures. Numerical benchmark examples are presented to demonstrate the effectiveness of the present approach.

Acknowledgement

References

Adams, T., Giani, S. and Coombs, W. (2016) Topology optimisation using level set methods and the discontinuous Galerkin method. In: *Proc. of the 24th UK Conf. of the Association for Computational Mechanics in Engineering (ACME-UK)*, Cardiff University, Cardiff: 6–9.

Allaire, G., de Gournay, F., Jouve, F. and Toader, A. M. (2005) Structural optimization using topological and shape sensitivity via a level set method. *Control Cybernet.* **34**, 59–80.

Allaire, G., Jouve, F. and Toader, A. M. (2004) Structural optimization using sensitivity analysis and a level-set method. *J. Comput. Phys.* 194 363–393.
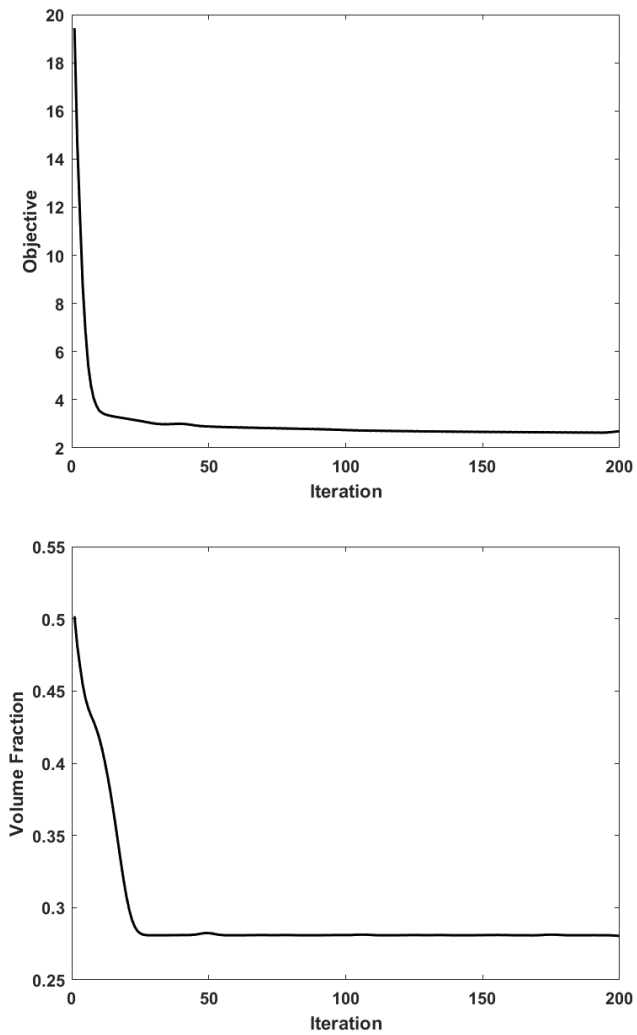
Figure 13: Convergence history of the objective (top) and volume fraction (bottom) values for Example 4.
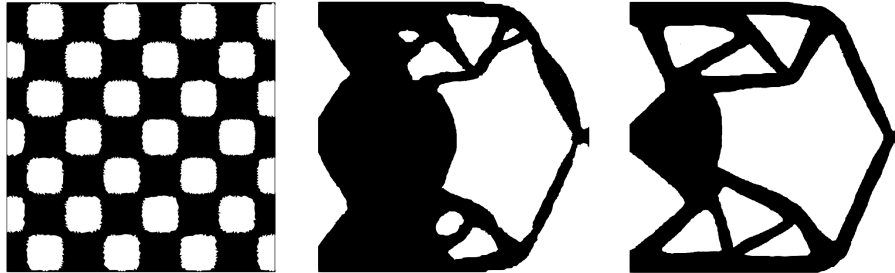
Figure 14: Initial design, Iteration=20 and final design from left to right for Example 5: nonlinear elasticity

ALLAIRE, G., DAPOGNY, C. AND JOUVE, F. (2021) Shape and topology optimization. *Handb. Numer. Anal.* 22, 1–132.

ARNOLD, D. N., BREZZI, F., COCKBURN, B. AND MARINI, L. D. (2002) Unified analysis of discontinuous Galerkin methods for elliptic problems. *SIAM J. Numer. Anal.* 39, 1749–1779.

BENDSØE, M. P. AND SIGMUND, O. (2003) *Topology Optimization: Theory, Methods, and Applications.* Springer, Berlin.

BUHL, T., PEDERSEN, C. AND SIGMUND, O. (2000) Stiffness design of geometrically nonlinear structures using topology optimization. *Struct. Multidiscip. Optim.* **19** (2) 93–104.

CIARLET, P. G. (1988) *Mathematical Elasticity, Three-Dimensional Elasticity, vol. I.* North-Holland, Amsterdam.

DAPOGNY, C. AND FREY, P. (2010) Computation of the signed distance function to a discrete contour on adapted triangulation. *Calcolo*, 49 1-27.

ERN, A. AND GUERMOND, J. L. (2006) Discontinuous Galerkin methods for Friedrichs' systems. I. General theory. *SIAM J. Numer. Anal.* 44, 753–778.

EVGRAFOV, A. (2018) Discontinuous Petrov-Galerkin methods for topology optimization. In: H. Rodrigues et al., eds., *Proceedings of the 6th International Conference on Engineering Optimization. EngOpt 2018.* Springer, Cham.

FULMANSKI, P., LAURAIN, A., SCHEID, J.-F. AND SOKOŁOWSKI, J. (2008) Level set method with topological derivatives in shape optimization. *Int. J. Comput. Math.* 85, 1491–1514.

GANGHOFFER, J. F., PLOTNIKOV, P. I. AND SOKOLOWSKI, J. (2018) Nonconvex model of material growth: mathematical theory. *Arch. Rational Mech. Anal.* 230, 839–910.
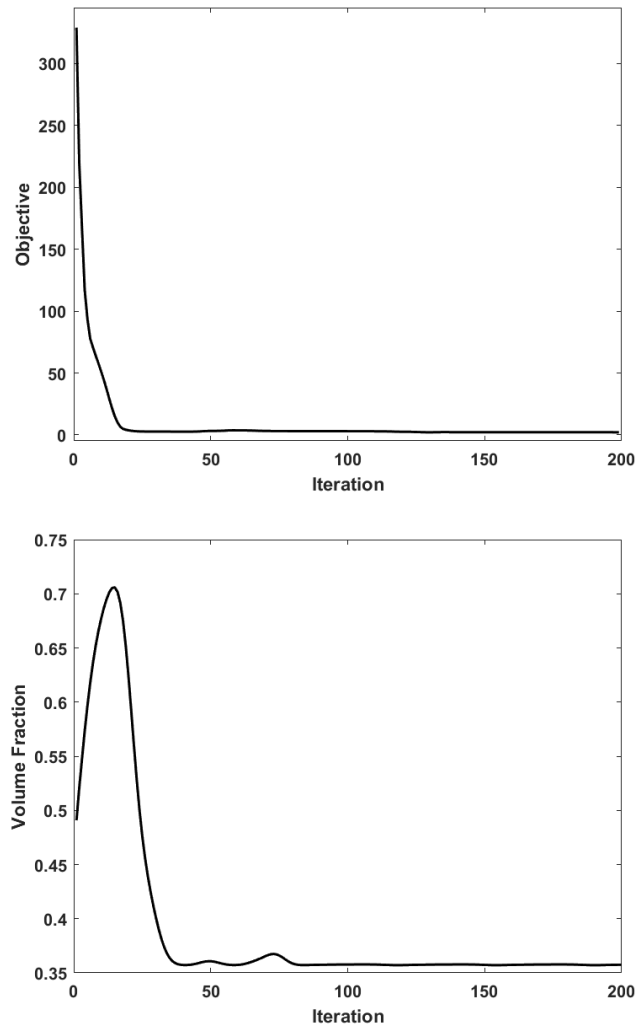
Figure 15: Convergence histories of the objective (top) and volume fraction (bottom) values for Example 5

HANSBO, P. AND LARSON, M. G. (2022) Augmented Lagrangian approach to deriving discontinuous Galerkin methods for nonlinear elasticity problems. *Int. J. Numer. Methods Eng.* 123, 4407–4421.

HECHT, F. (2012) New development in FreeFem++. *J. Numer. Math.* 20, 251–265.

HOWELL, L. L. (2001) *Compliant Mechanisms.* John Wiley & Sons.

KIM, N.-H. (2015) *Introduction to Nonlinear Finite Element Analysis.* Springer, US.

KWAK, J. AND CHO, S. (2005) Topological shape optimization of geometrically nonlinear structures using level set method. *Comput. Struct.* 83, 2257–2268.

LAURAIN, A. (2018) A level set-based structural optimization code using FEniCS. *Struct. Multidisc. Optim.* 58, 1311–1334.

NOVOTNY, A. A. AND SOKOŁOWSKI, J. (2013) *Topological Derivatives in Shape Optimization.* Springer, Berlin.

NOVOTNY, A. A., SOKOŁOWSKI, J. AND ŻOCHOWSKI, A. (2019) *Applications of the Topological Derivative Method.* Springer, Cham.

OSHER, S. AND SETHIAN, J. A. (1988) Front propagation with curvature dependent speed: Algorithms based on Hamilton-Jacobi formulations. *J. Comput. Phys.* 79, 12–49.

QIAN, M. AND ZHU, S. (2022) A level set method for Laplacian eigenvalue optimization subject to geometric constraints. *Comput. Optim. Appl.* 82, 499–524.

RIVIÈRE, B., SHAW, S., WHEELER, M. F. AND WHITEMAN, J. R. (2003) Discontinuous Galerkin finite element methods for linear elasticity and quasistatic linear viscoelasticity. *Numer. Math.* 95, 347–376.

SOKOŁOWSKI, J. AND ZOLÉSIO, J. P. (1992) *Introduction to Shape Optimization: Shape Sensitivity Analysis.* Springer, Heidelberg.

TAN, Y. AND ZHU, S. (2023) A discontinuous Galerkin level set method using distributed shape gradient and topological derivatives for multi-material structural topology optimization. *Struct. Multidiscip. Optim.* 66; Article number: 170.

TAN, Y. AND ZHU, S. (2024) Numerical shape reconstruction for a semi-linear elliptic interface inverse problem. *East Asian J. Appl. Math.* 14, 147–178.

ZHENG, J., ZHU, S. AND SOLEYMANI, F. (2024) A new efficient parametric level set method based on radial basis function-finite difference for structural topology optimization. *Comput. Struct.* 291, 107364.

ZHU, S., HU, X. AND WU, Q. (2018) A level set method for shape optimization in semilinear elliptic problems. *J. Comput. Phys.* 355, 104–120.